A room-temperature semiconductor spaser operating near 1.5 μm

R. A. Flynn,[1] C. S. Kim,[1] I. Vurgaftman,[1] M. Kim,[1] J. R. Meyer,[1] A. J. Mäkinen,[1] K. Bussmann,[2] L. Cheng,[3] F.-S. Choa,[3] and J. P. Long[4,*]

[1]*Optical Sciences Division, Naval Research Laboratory, Washington, DC 20375, USA*
[2]*Materials Science and Technology Division, Naval Research Laboratory, Washington, DC 20375, USA*
[3]*Department of Electrical Engineering, University of Maryland Baltimore County, Baltimore, Maryland 21250, USA*
[4]*Chemistry Division, Naval Research Laboratory, Washington, DC 20375, USA*
**jp.long@nrl.navy.mil*

Abstract: Room temperature spasing of surface plasmon polaritons at 1.46 μm wavelength has been demonstrated by sandwiching a gold-film plasmonic waveguide between optically pumped InGaAs quantum-well gain media. The spaser exhibits gain narrowing, the expected transverse-magnetic polarization, and mirror feedback provided by cleaved facets in a 1-mm long cavity fabricated with a flip-chip approach. The 1.06-μm pump-threshold of ~60 kW/cm^2 is in good agreement with calculations. The architecture is readily adaptable to all-electrical operation on an integrated microchip.

OCIS codes: (130.3120) Integrated optics devices; (230.6080) Sources; (240.6680) Surface plasmons.

References and links

1. S. A. Maier and H. A. Atwater, "Plasmonics: localization and guiding of electromagnetic energy in metal/dielectric structures," J. Appl. Phys. **98**(1), 011101 (2005).
2. P. L. Stiles, J. A. Dieringer, N. C. Shah, and R. P. Van Duyne, "Surface-enhanced Raman spectroscopy," Annu Rev Anal Chem (Palo Alto Calif) **1**(1), 601–626 (2008).
3. P. Genevet, J. P. Tetienne, E. Gatzogiannis, R. Blanchard, M. A. Kats, M. O. Scully, and F. Capasso, "Large enhancement of nonlinear optical phenomena by plasmonic nanocavity gratings," Nano Lett. **10**(12), 4880–4883 (2010).
4. D. E. Chang, A. S. Sorensen, E. A. Demler, and M. D. Lukin, "A single-photon transistor using nanoscale surface plasmons," Nat. Phys. **3**(11), 807–812 (2007).
5. C.-S. Kim, I. Vurgaftman, R. A. Flynn, M. Kim, J. R. Lindle, W. W. Bewley, K. Bussmann, J. R. Meyer, and J. P. Long, "An integrated surface-plasmon source," Opt. Express **18**(10), 10609–10615 (2010).
6. D. J. Bergman and M. I. Stockman, "Surface plasmon amplification by stimulated emission of radiation: quantum generation of coherent surface plasmons in nanosystems," Phys. Rev. Lett. **90**(2), 027402 (2003).
7. M. I. Stockman, "Spasers explained," Nat. Photonics **2**(6), 327–329 (2008).
8. M. T. Hill, M. Marell, E. S. P. Leong, B. Smalbrugge, Y. Zhu, M. Sun, P. J. van Veldhoven, E. J. Geluk, F. Karouta, Y.-S. Oei, R. Nötzel, C.-Z. Ning, and M. K. Smit, "Lasing in metal-insulator-metal sub-wavelength plasmonic waveguides," Opt. Express **17**(13), 11107–11112 (2009).
9. R. F. Oulton, V. J. Sorger, T. Zentgraf, R.-M. Ma, C. Gladden, L. Dai, G. Bartal, and X. Zhang, "Plasmon lasers at deep subwavelength scale," Nature **461**(7264), 629–632 (2009).
10. R.-M. Ma, R. F. Oulton, V. J. Sorger, G. Bartal, and X. Zhang, "Room-temperature sub-diffraction-limited plasmon laser by total internal reflection," Nat. Mater. **10**(2), 110–113 (2011).
11. M. A. Noginov, G. Zhu, A. M. Belgrave, R. Bakker, V. M. Shalaev, E. E. Narimanov, S. Stout, E. Herz, T. Suteewong, and U. Wiesner, "Demonstration of a spaser-based nanolaser," Nature **460**(7259), 1110–1112 (2009).
12. I. De Leon and P. Berini, "Amplification of long-range surface plasmons by a dipolar gain medium," Nat. Photonics **4**(6), 382–387 (2010).
13. M. C. Gather, K. Meerholz, N. Danz, and K. Leosson, "Net optical gain in a plasmonic waveguide embedded in a fluorescent polymer," Nat. Photonics **4**(7), 457–461 (2010).
14. A. Banerjee, R. Li, and H. Grebel, "Surface plasmon lasers with quantum dots as gain media," Appl. Phys. Lett. **95**(25), 251106 (2009).
15. G. Veronis and S. Fan, "Theoretical investigation of compact couplers between dielectric slab waveguides and two-dimensional metal-dielectric-metal plasmonic waveguides," Opt. Express **15**(3), 1211–1221 (2007).
16. M. Bahriz, V. Moreau, J. Palomo, R. Colombelli, D. A. Austin, J. W. Cockburn, L. R. Wilson, A. B. Krysa, and J. S. Roberts, "Room-temperature operation of lambda=7.5 μm surface-plasmon quantum cascade lasers," Appl. Phys. Lett. **88**(18), 181103 (2006).

#143652 - $15.00 USD Received 4 Mar 2011; revised 8 Apr 2011; accepted 16 Apr 2011; published 22 Apr 2011

Report Documentation Page

Form Approved
OMB No. 0704-0188

1. REPORT DATE	2. REPORT TYPE	3. DATES COVERED
APR 2011		**00-00-2011 to 00-00-2011**

4. TITLE AND SUBTITLE	5a. CONTRACT NUMBER
A Room-Temperature Semiconductor Spaser Operating Near 1.5 μm	5b. GRANT NUMBER
	5c. PROGRAM ELEMENT NUMBER
6. AUTHOR(S)	5d. PROJECT NUMBER
	5e. TASK NUMBER
	5f. WORK UNIT NUMBER
7. PERFORMING ORGANIZATION NAME(S) AND ADDRESS(ES) **Naval Research Laboratory,Materials Science and Technology Division,Washington,DC,20375**	8. PERFORMING ORGANIZATION REPORT NUMBER
9. SPONSORING/MONITORING AGENCY NAME(S) AND ADDRESS(ES)	10. SPONSOR/MONITOR'S ACRONYM(S)
	11. SPONSOR/MONITOR'S REPORT NUMBER(S)

12. DISTRIBUTION/AVAILABILITY STATEMENT
Approved for public release; distribution unlimited

13. SUPPLEMENTARY NOTES
Optics Express, Vol. 19, Issue 9, pp. 8954-8961 April 25, 2011,Government or Federal Purpose Rights License

14. ABSTRACT
Room temperature spasing of surface plasmon polaritons at 1.46 μm wavelength has been demonstrated by sandwiching a gold-film plasmonic waveguide between optically pumped InGaAs quantum-well gain media. The spaser exhibits gain narrowing, the expected transverse-magnetic polarization, and mirror feedback provided by cleaved facets in a 1-mm long cavity fabricated with a flip-chip approach. The 1.06-μm pump-threshold of ~60 kW/cm2 is in good agreement with calculations. The architecture is readily adaptable to all-electrical operation on an integrated microchip.

15. SUBJECT TERMS

16. SECURITY CLASSIFICATION OF:			17. LIMITATION OF ABSTRACT	18. NUMBER OF PAGES	19a. NAME OF RESPONSIBLE PERSON
a. REPORT	b. ABSTRACT	c. THIS PAGE			
unclassified	**unclassified**	**unclassified**	**Same as Report (SAR)**	**9**	

17. A. Bousseksou, R. Colombelli, A. Babuty, Y. De Wilde, Y. Chassagneux, C. Sirtori, G. Patriarche, G. Beaudoin, and I. Sagnes, "A semiconductor laser device for the generation of surface-plasmons upon electrical injection," Opt. Express **17**(11), 9391–9400 (2009).
18. A. Babuty, A. Bousseksou, J.-P. Tetienne, I. M. Doyen, C. Sirtori, G. Beaudoin, I. Sagnes, Y. De Wilde, and R. Colombelli, "Semiconductor surface plasmon sources," Phys. Rev. Lett. **104**(22), 226806 (2010).
19. D. Sarid, "Long-range surface-plasma waves on very thin metal films," Phys. Rev. Lett. **47**(26), 1927–1930 (1981).
20. B. Jensen and A. Torabi, "Refractive index of quaternary $In_{1-x}Ga_xAs_yP_{1-y}$ lattice matched to InP," J. Appl. Phys. **54**(6), 3623–3625 (1983).
21. G. Jones, A. D. Smith, E. P. O'Reilly, M. Silver, A. T. R. Briggs, M. J. Fice, A. R. Adams, P. D. Greene, K. Scarrott, and A. Vranic, "The influence of tensile strain on differential gain and Auger recombination in 1.5-μm multiple-quantum-well lasers," IEEE J. Quantum Electron. **34**(5), 822–833 (1998).
22. J. A. Dionne, L. Sweatlock, H. A. Atwater, and A. Polman, "Planar metal plasmon waveguides: frequency-dependent dispersion, propagation, localization, and loss beyond the free electron model," Phys. Rev. B **72**(7), 075405 (2005).
23. G. W. Ford and W. H. Weber, "Electromagnetic interactions of molecules with metal surfaces," Phys. Rep. **113**(4), 195–287 (1984).
24. R. A. Flynn, I. Vurgaftman, K. Bussmann, B. S. Simpkins, C.-S. Kim, and J. P. Long, "Transmission efficiency of surface plasmon polaritons across gaps in gold waveguides," Appl. Phys. Lett. **96**(11), 111101 (2010).
25. B.-S. Kim, Y. Chung, and J.-S. Lee, "An efficient split-step time-domain dynamic modeling of DFB/DBR laser diodes," IEEE J. Sel. Top. Quantum Electron. **36**(7), 787–794 (2000).
26. L. A. Coldren and S. W. Corzine, *Diode Lasers and Photonic Integrated Circuits* (Wiley, 1995).

1. Introduction

The field of plasmonics exploits the surface plasmon, a hybridized mode of conduction currents and optical fields confined to a metallic surface. Because these modes can be squeezed to nanoscale dimensions, plasmonics may ultimately lead to dense optical circuitry on par with electronic circuitry [1]. In addition, nanoconfined field enhancements provide a promising basis for advanced sensing (*e.g.*, surface enhanced Raman scattering [2]), low-power nonlinear optics [3], and quantum information schemes relying on strong optical interactions with qubits [4]. Many of these applications will require practical integrated sources able to launch SPPs onto plasmonic waveguides. While we recently demonstrated an on-chip source that converts laser-diode photons to SPPs [5], the direct generation of SPPs through stimulated emission in a spaser architecture is now widely pursued. The spaser is a laser analog wherein a proximal gain medium amplifies surface plasmons oscillating on a metallic structure [6,7]. However, it is challenging to generate gains sufficient to overcome the ohmic losses of plasmonically driven conduction currents. Nano-scale sources are desirable, but to date their high losses impose either low-temperature operation [8,9] or architectures incompatible with electrical driving [10,11]. Micro-scale sources [12–14] may be simpler to fabricate, and can in principle be coupled to nano-waveguides [15], but electrical excitation has so far been limited to the longwave IR (7.5 μm) where ohmic losses are reduced [16–18]. Here we demonstrate a room-temperature spaser operating within a standard communications band at 1.46 μm. The present demonstration proves the principle with optical pumping, a common first step in new laser technologies. However, our III-V semiconductor architecture provides a clear path to electrical operation and is adaptable to an integrated microchip source.

2. Spaser design and fabrication

By combining several strategies to reduce loss and maximize gain, as outlined in Fig. 1, we achieved room-temperature spasing at 1.46 μm for pumping levels corresponding to drive currents in the range of modern laser diodes. As in earlier demonstrations of gain using planar-film SPPs, which employed optically pumped laser-dye solutions [12] or fluorescent polymers [13], we reduced loss by exploiting the "long-range" SPP mode that propagates on an optically thin metal film sandwiched between two dielectrics with matched refractive indices [19]. To ensure the perfect matching that avoids the possibility of mode cut-off, we enclosed the Au film between top and bottom dies cleaved from the same InP growth wafer, and then solder-bonded the dies in a flip-chip arrangement (Fig. 1). We reduced losses further by using an ultra-thin (15-nm) Au film to decrease the SPP mode overlap with the lossy metal.

#143652 - $15.00 USD Received 4 Mar 2011; revised 8 Apr 2011; accepted 16 Apr 2011; published 22 Apr 2011

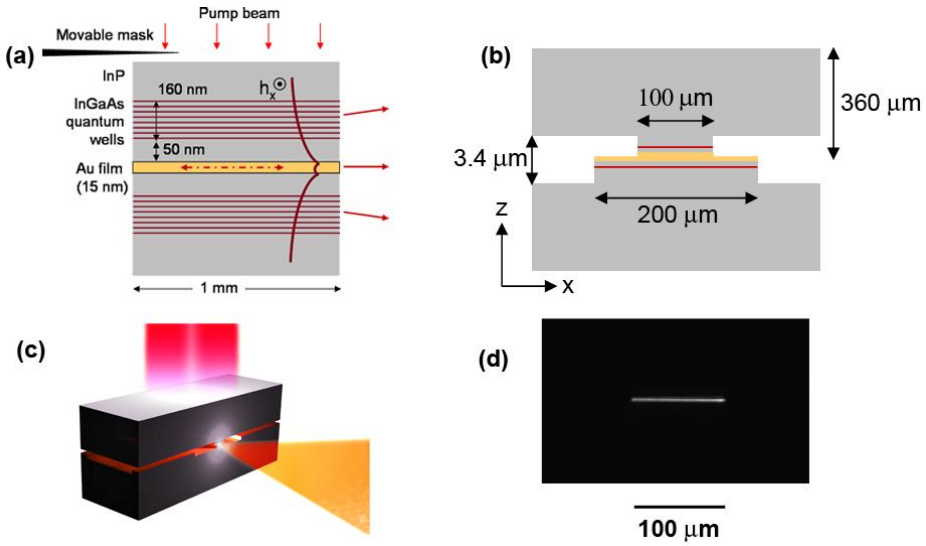

Fig. 1. (a) Side view (not to scale), showing the Au-film plasmonic waveguide sandwiched between two dies containing the QW stacks. The stacks are immersed in the evanescent field of the long-range SPP mode represented by the transverse optical magnetic field h_x. Arrows to the right indicate the diagnostic radiation emitted when SPPs reflect from the end facet. (b) End-on view (not to scale) showing the ridge architecture after dies are flip-chip bonded. (c) Rendering of the bonded dies pumped from above and emitting diagnostic radiation to the right. (d) End-on micrograph of the output facet, showing above-threshold diagnostic radiation at 1.46 μm emitted from the end of the SPP waveguide over the width of 100-μm-wide confining ridge. Output power was obtained by integrating the calibrated micrograph intensity.

The optical gain was enhanced by distributing eight quantum wells (QWs) on each side of the Au film throughout the long-range SPP mode profile, which we computed with transfer-matrix methods (see Section A.2) and appropriate refractive indices [20] to extend ~150 nm on each side of the Au film [Fig. 1(a)]. In addition, optical gain for the transverse-magnetic (TM) polarized SPP mode was obtained by introducing tensile strain in the QWs, compensated by compressive strain in the barriers [21]. Figure 1(a) depicts schematically the modal extent by showing the optical magnetic field amplitude h_x for the symmetric long-range mode. Not shown is the high-loss antisymmetric mode that is more tightly confined near the film [19,22]. A 50-nm-thick InP spacer layer, placed between the closest QWs and the Au film, avoids coupling to the lossy mode, and also minimizes the deleterious quenching of photoexcited electron-hole pairs to nonradiative modes in the Au [13,23]. Transfer-matrix calculations indicate that since the epitaxial structure does not incorporate any guiding or cladding layers and the QW index contrast is rather low, only SPP modes conforming to the symmetric and asymmetric character described above exist, though these SPPs constitute a large number of transverse modes circulating between the end mirrors (see Section A.2).

As described more thoroughly in Section A.1, the spaser was fabricated by etching 1.7-μm-high ridges through the QWs on each of two coupons cleaved from the 360-μm thick growth wafer. One ridge of width 100 μm laterally confined the SPP modes, while the second 200-μm-wide ridge seated the first as shown in Fig. 1(b). After evaporating an ultrathin 7.5-nm Au film onto each coupon, they were cleaved into matching dies that were then flip-chip bonded to form a Fabry-Perot cavity of length 1 mm and width 100 μm [Fig. 1(c)]. The QWs were pumped at 1.06 μm with 140 ns pulses (full-width-half-maximum) as described in Section A.1. The spaser was characterized by measuring the intensity of micrographs of the free-space radiation (1.46 μm) emitted from the cavity output-facet when SPPs encountered the end of the Au waveguide [5,24]. Figure 1(d) shows a typical micrograph taken above the spasing threshold with our custom IR microscope. The resolution-limited line replicates the 100-μm ridge width and coincides with the location of the Au film.

#143652 - $15.00 USD Received 4 Mar 2011; revised 8 Apr 2011; accepted 16 Apr 2011; published 22 Apr 2011

3. Results and discussion

Spaser output as a function of peak pump intensity is plotted in Fig. 2 (the light-light, or "L-L" curve). An inset with linear scale shows that the output increases quasi-linearly above a clear threshold near 60 kW/cm^2, following classic laser behavior. The maximum detected energy of ~5 nJ per pulse corresponds to a peak power of ~26 mW. Comparison in the main figure with the L-L curve for a control device comprising only one of the processed Au-coated dies, for which the dielectric asymmetry extinguishes the long-range SPP mode, supports the conclusion that the spaser characteristic is not due to an inadvertent lasing mode.

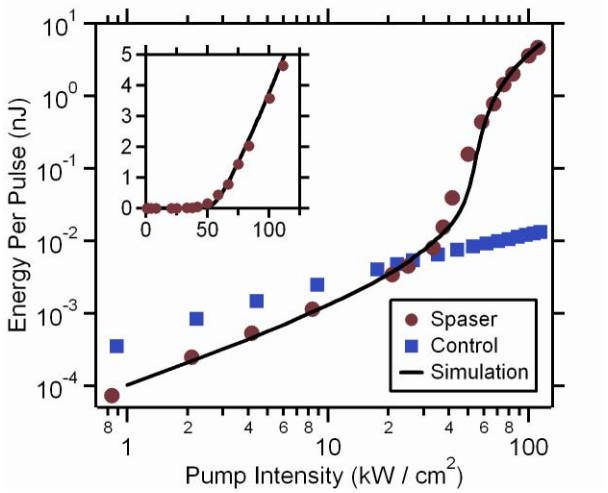

Fig. 2. Log-log plot comparing the strength of diagnostic radiation from the spaser (circles) and a control device with air above the Au-film waveguide (squares) *vs* the instantaneous pump-intensity. The control exhibited only spontaneous emission. Solid line shows expectations from our wave-equation model. Inset: L-L plot with linear axes showing threshold at ~60 kW/cm^2 pump.

The theoretical L-L curve of Fig. 2, based on a spaser wave-propagation analysis described below, agrees well with the measurements. The output polarization of the image of Fig. 1(d) was assessed with a rotating polarization filter in the microscope. Figure 3(a) shows that the output above threshold was strongly TM polarized, *i.e.*, with the optical magnetic field parallel to the plane of the Au film. Since the output polarization maps that of the originating mode [5], the strong TM polarization above threshold provides further evidence that the emission originates from gain in the strictly TM-polarized SPP channel. In contrast, below threshold, the emission forming the image was nominally unpolarized, which is attributable to the presence of TE-polarized QW photoluminescence (PL) within the microscope depth-of-field contributing comparably to TM-polarized PL and weak below-threshold SPP emission. Finally, the rapid narrowing of the output spectrum as the spaser passes through threshold, Fig. 3(b), gives additional evidence of spasing by analogy to laser behavior.

#143652 - $15.00 USD Received 4 Mar 2011; revised 8 Apr 2011; accepted 16 Apr 2011; published 22 Apr 2011

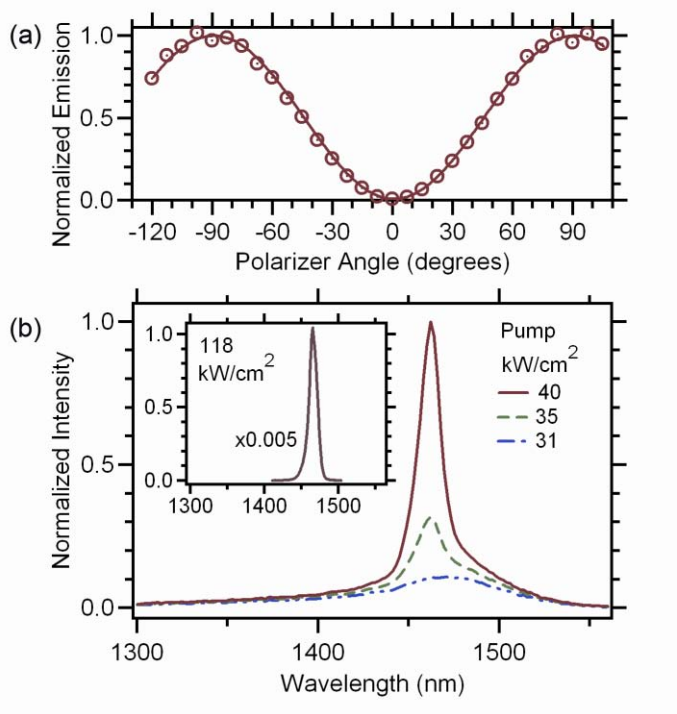

Fig. 3. (a) Polarization of the emitted diagnostic radiation (111 kW/cm^2 pump intensity) measured with a rotating polarizing filter, showing maxima consistent with TM polarized SPPs. (b) Spectral narrowing as the pump is varied through threshold. Inset: Spectrum at 118 kW/cm^2, near our highest pump intensity.

As described more fully in Section A.2, spaser operation was modeled by numerically solving one-dimensional (1D) wave equations for two SPPs counter-propagating along the cavity axis [25], coupled to the rate equations for electron and hole generation and recombination in the QWs [26]. The two SPP waves were coupled by reflections at each facet, the reflectance of which was computed with finite element methods. The detected power was determined from the steady-state power circulating internally by accounting for facet reflectance, integrating over the measured pump-laser pulse shape, and correcting for the fraction of radiation intercepted by the objective.

Fitting the slope efficiency above threshold in the L-L curve of Fig. 2 implies an internal loss of ~720 cm^{-1}, as compared to the computed value of 45 cm^{-1} based on the optical constants of Au (Section A.2). Such a large apparent loss could be due to scattering at voids or other defects in the Au films if the two dies bonded imperfectly. For definiteness, our simulations assume the extra loss to be uniform, although it may well be inhomogeneous. If the loss indeed arises from processing imperfections, future improvements may considerably enhance the spaser performance. The other fitting parameter, besides the loss, is the pump light absorbed in the QWs. The derived value of 18% for the top set of QWs is close to that expected based on the calculated absorption coefficient at the pump wavelength and accounting for reflection at the initial substrate interface. With additional absorption in the metal film, we expect the bottom set of QWs to absorb only 5.3% of the incident intensity. While these different levels of pumping in the two sets of QWs disturb the desired symmetry of the index of refraction n, detailed calculations estimate a maximal Δn~0.02, which we compute affects the internal loss and confinement factor negligibly. Finally, in fitting the L-L curve *below* threshold, where 1D spaser oscillation no longer dominates, we reduced the spontaneous-emission coupling factor to account for the fact that SPPs spontaneously emitted

#143652 - $15.00 USD Received 4 Mar 2011; revised 8 Apr 2011; accepted 16 Apr 2011; published 22 Apr 2011

into the Au film propagate two dimensionally, so most were not collected at the objective aperture.

To test whether feedback within the spaser cavity, as opposed to amplified spontaneous emission (ASE), dominates the observed SPP generation, we recorded the front-facet output while scanning a knife-edge mask to progressively block the pump laser, as sketched in Fig. 1(a). The resulting output is plotted in Fig. 4 for a series of pump intensities. Above threshold, we observe three distinct regions of behavior, which may be identified by comparing with the wave-propagation model. In the first region (marked as 1 in Fig. 4), the output drops precipitously as the mask begins to shade the rear facet, clearly indicating a suppression of the spaser oscillation by SPP absorption in the masked (unpumped) region. In the relatively flat plateau at intermediate mask positions (region 2), ASE dominates the emission, but is saturated due to the large propagation distance to the output facet. Finally, as the mask nears the output facet and the gain × path-length product decreases (region 3), the generated ASE decreases exponentially. For pump intensities well below threshold (25 kW/cm^2), no gain is present, and a flat spontaneous-emission curve is observed.

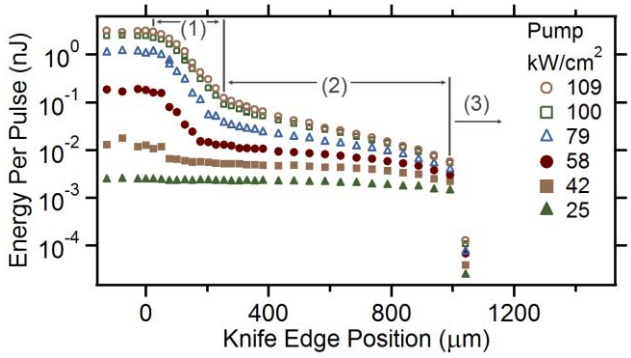

Fig. 4. Front-facet emission as a knife-edge mask blocking the pump light is scanned from back to front facets [as sketched in Fig. 1(a)], for various pump intensities. The three regions identified with simulations are: (1) rapid falloff (0 to ~200 μm) as SPP absorption in the mask shadow prevents back-facet feedback; (2) a plateau (to ~950 μm) where saturated amplified-spontaneous-emission dominates; and (3) exponential falloff of unsaturated ASE.

4. Summary

In conclusion, by extending laser-diode technology, we have demonstrated an optically pumped spaser capable of generating >25 mW of external peak power from SPP-radiation conversion. Important advantages of our design include room temperature operation near a communication wavelength and an architecture suitable for extension to all-electrical operation. Simulations reproduce all the salient characteristics, and also indicate that significant power enhancement and threshold reduction may become possible with better Au-film quality and bonding. If such improvements can reduce plasmonic losses to the intrinsic ohmic level, the extrapolation of our device performance to an electrically driven spaser implies the potential for a threshold of ~500 A/cm^2, only slightly more than modern laser diodes in this wavelength range. With further streamlining through reduced ridge-width and cavity length, this source could then be employed in passive or active plasmonic circuitry.

Appendix A

A.1 Fabrication and characterization

The spaser was produced from a 360-μm-thick InP wafer on which eight 10-nm thick quantum wells ($In_{0.39}Ga_{0.61}As$), with 10-nm barrier layers ($In_{0.67}Al_{0.33}As$), were grown by metalorganic chemical-vapor deposition. The composition imparted tensile strain to the QWs, compensated by compressive strain in the barriers, to favor TM-polarized gain over TE-

#143652 - $15.00 USD Received 4 Mar 2011; revised 8 Apr 2011; accepted 16 Apr 2011; published 22 Apr 2011

polarized gain [21], a key to achieving spasing in the TM-polarized SPP mode. To prevent coupling to the highly confined and lossy anti-symmetric SPP mode, and to prevent quenching of electron-hole pairs to the Au film, the QWs were buried by a final 50-nm InP capping layer. Coupons were then cleaved from the wafer and reactive-ion etched to a depth of 1.7 μm in two patterns, one for each die, to define the 100-μm ridge on the first die for laterally confining the SPPs, the 200-μm-wide ridge on the second die for seating the 100-μm ridge, and wells to accommodate the Sn-Pb solder used for bonding the dies. Each coupon was then transferred to ultrahigh vacuum for thermal evaporation of 7.5-nm of Au directly onto the InP capping layer. Depositing Au films onto both coupons is expected to promote bonding. Film thickness was calibrated by atomic force microscopy and verified with x-ray fluorescence. To prevent islanding of the ultrathin films, substrates were cooled to 87 K during evaporation, yielding nano-domained films with 0.3 nm RMS roughness over 1 μm^2. Finally, two dies were cleaved from the patterned coupons, and aligned and bonded with pressure and heat in a commercial flip chip bonder (Finetech).

The spaser was pumped with a Q-switched Nd:YAG laser (cw-pumped, 1.06 μm wavelength, pulse duration 140 ns full-width-half-maximum, 25 Hz repetition rate). The pump beam was weakly focused to a ~1.2 x 3.5 mm^2 spot to overfill the 100 μm x 1 mm cavity. Pump intensity over the cavity varied by less than ±6% as determined with an imaging beam profiler. Spaser output was determined by measuring micrographs obtained with a charge-coupled-device camera (Xenics, Inc.) mated to a custom microscope equipped with an infrared objective (Mitutoyo, 0.65 numerical aperture), a rotatable polarizing filter, a pump-laser rejection filter, and calibrated neutral density filters.

A.2 Theoretical modeling

The SPP mode at 1.46 μm was designed using the transfer-matrix method with suitable semiconductor indices of refraction [20] and a Au dielectric constant of −96.9 + i6.13 derived from ellipsometric measurements of evaporated Au films. The resulting mode exhibits a low theoretical ohmic loss of 45 cm^{-1}. The mode extends exponentially into the dielectric environment with a characteristic decay height of ~150 nm, to provide a large confinement factor of 23.5% for each set of multiple QWs. (The large 360-μm-thick wafers ensure that any guided photonic mode within a die has negligible overlap and is ignored). Because of the large 100 μm width of the active ridge, in fact many SPP guided modes with different transverse character similarly overlap the QWs and contribute. However, as these modes exhibit very similar vertical field profiles, they can be treated within a one-dimensional (1D) calculation, as is commonly done for wide-ridge lasers. Hence, the spaser was modeled by numerically solving 1D wave equations for two waves counter-propagating along the cavity axis and coupled by facet reflections [25]. During each time step and location along the axis, each wave was propagated over a cell with gain and spontaneous-emission characteristics determined by separate rate equations for the carrier densities in the QWs above and below the Au film. The facet reflectances R were obtained from finite-element analysis (COMSOL). Assuming perfect alignment of the cleaved ends of the top and bottom dies (measured offset < 1 μm), $R = 0.27$ was derived for the "front" output facet, whereas $R = 0.07$ was calculated for the rear facet with measured offset 20 μm. A standard model of QW characteristics [26] computed the gain as a function of pumped carrier-density and the radiative recombination coefficient (5 x 10^{-11} cm^3/s). An Auger coefficient of 4 x 10^{-29} cm^6/s was inferred from a comparison of the gains and the measured threshold current densities of conventional lasers with similar QWs [21]. The Ford-Weber model [23] was used to estimate that ≈21% of the total QW spontaneous-emission into both light- and heavy-hole states was coupled into the long-range SPP mode, and that the total emission rate (*i.e.*, into both SPPs and photons) was enhanced by 28% compared to QWs embedded in bulk InP. The SPP propagation loss was treated as a parameter to fit the slope efficiency above threshold, neglecting the weak free-carrier absorption in the QWs.

#143652 - $15.00 USD Received 4 Mar 2011; revised 8 Apr 2011; accepted 16 Apr 2011; published 22 Apr 2011

To find the internally circulating SPP power, the 1D model described above was iterated to steady state and then integrated over the measured pump pulse-shape. Computation of the externally collected power accounted for the Fabry-Perot cavity facet transmission and the finite angular acceptance of the objective, which collected ~94% of the far-field radiation pattern diffracting from the SPP mode profile. Below threshold, where 1D spaser oscillation is no longer supported by gain and end-facet feedback, SPP generation occurs through spontaneous emission into the 2D continuum of SPP modes. The 2D character necessitates accounting for an additional loss of detected power because, neglecting any SPP reflection from the ridge sidewalls, only ~7% of the 2D SPP population travels in a cone (11.7° internal half-angle) that can externally radiate into the objective's acceptance aperture of 40.5° after refracting at the output facet. Similarly, while the 1D model captures the salient qualitative features of the movable-mask data of Fig. 4, it is unable to reproduce some of the quantitative details because ASE into 2D modes governs the device once the rear facet is shaded.

Acknowledgments

This work was funded by the Office of Naval Research. The research was performed while R. A. Flynn held a National Research Council Associateship at the Naval Research Laboratory Chemistry Division.

#143652 - $15.00 USD Received 4 Mar 2011; revised 8 Apr 2011; accepted 16 Apr 2011; published 22 Apr 2011